AIAA JOURNAL
Vol. 30, No. 2, February 1992

Effect of Dropped Plies on the Strength of Graphite-Epoxy Laminates

James M. Curry*
Rohr Industries, Inc., Chula Vista, California 92012
Eric R. Johnson†
Virginia Polytechnic Institute and State University, Blacksburg, Virginia 24061
and
James H. Starnes Jr.‡
NASA Langley Research Center, Hampton, Virginia 23665

The reduction in the compressive and tensile strength of graphite-epoxy laminates with thickness discontinuities due to dropped plies was studied by experiment and analysis. The specimens were fabricated with all the dropped plies lumped together in the center of a 16-ply quasi-isotropic layup, such that one surface was flat and the slope of the opposite surface changed abruptly at the dropped ply location to accommodate the thickness change. Even though the thick and thin sections are symmetrically laminated, there exists bending-extension coupling due to the geometric eccentricity of the middle planes of the thick and thin sections. Results from tests on 37 specimens are reported that differed in the configuration of the dropped plies only. The axial strength of a laminate with dropped plies is less than the strength of its thin section, and the compressive strength of a laminate with dropped plies is less than its tensile strength. The reduction in axial strength is directly related to the axial stiffness change between the thick and thin sections. To examine the mechanism of failure, the three-dimensional state of stress in the dropped ply region was evaluated by the finite element method. A tensile interlaminar criterion predicted the correct location of failure, but underestimated the failure load, and therefore is a conservative analysis procedure for design.

Nomenclature

b = laminate width
N_x = normal stress resultant acting on the longitudinal face; positive in tension, negative in compression
t_1, t_2 = thicknesses of the laminate's thick section and thin section, respectively
U, V, W = unknown portions of the displacements in Eqs. (1–3)
u, v, w = longitudinal, width-wise, and thickness direction displacement components, respectively
x, y, z = right-handed Cartesian coordinate system with the x-axis along the longitudinal direction of the laminate, the y-axis along the width, and the z-axis along the thickness direction; $x = 0$ at the end of the dropped plies
$\gamma_{yz}, \gamma_{zx}, \gamma_{xy}$ = engineering shear strain components
$\varepsilon_x, \varepsilon_y, \varepsilon_z$ = normal strain components
ε_y^0 = prescribed width-wise normal strain
κ_y, κ_{xy} = prescribed width-wise curvature and twist curvature, respectively

Introduction

THE dropped-ply configuration is a common design detail in laminated structures fabricated from fiber-reinforced composite materials. Internal plies are terminated at various spanwise locations on a wing skin to tailor a reduction in stiffness from root to tip, for example. Also, plies may be inserted in a laminate at joints to strengthen the joint, or inserted locally in a panel to act as a stiffener. Dropped plies result in an abrupt change of thickness and, consequently, produce a concentration of stress. Potential benefits in tailoring the stiffness by dropping plies in a composite structure may be compromised by a premature failure due to stress concentrations at the dropped-ply location.

Few references exist in the open literature on the dropped-ply problem. In Ref. 1 Kemp and Johnson presented a finite element analysis based on generalized plane deformation anisotropic elasticity.[2] The analysis was used to predict the three-dimensional state of stress in eight-ply laminates containing up to three dropped plies. Interlaminar stresses were found to be significant at the dropped-ply thickness discontinuity and, in many cases, the delamination criterion used predicted failure initiation before first ply failure. Reference 1 lacked a set of experiments to complement the analysis, and this motivated the present study.

An experimental and analytical study of a 30-ply laminate, typical of a wing skin, that contained two dropped plies at different locations through the thickness was performed by Adams et al.[3] The tests and analysis showed little strength reduction due to the dropped plies.

The objectives of this study are to quantify the effects of the number of plies dropped at a laminate thickness discontinuity, and the orientation of the dropped plies, on a laminate's tensile and compressive strengths, and to study the

Presented as Paper 87-0874 at the AIAA/ASME/ASCE/AHS 28th Structures, Structural Dynamics, and Materials Conference, Monterey, CA, April 6–8, 1987; received March 22, 1988; revision received May 6, 1991; accepted for publication June 11, 1991.

*Research Engineer. Member AIAA.
†Associate Professor. Member AIAA.
‡Head, Aircraft Structures Branch, Structural Mechanics Division. Fellow AIAA.

mechanisms of failure. To achieve these objectives an experimental program was conducted to study uniaxially loaded graphite-epoxy laminates with various dropped-ply geometries. Also, the finite element code developed in Ref. 1 was extended and refined to analyze the test specimens in this study. Although terminating many plies at one location may not be normally done in practice, the focus of this study is to quantify and understand the influence of the parameters affecting strength reduction for a single termination site.

Experiments

Specimens and Fixtures

The test specimens were made from AS4/3502 graphite-epoxy unidirectional tape manufactured by Hercules Inc. All specimens were 25.4 cm long, and either 2.54, 3.81, or 7.62 cm wide. Sublaminates consisting of either two, four, or eight plies were terminated at the midplane of the thick section. A photomicrograph of a specimen's edge at the dropped-ply location is shown in Fig. 1. This laminate has a transition from 20 plies in the thick section to 16 plies in the thin section with a group of four plies terminated at the midplane of the thick section. For the specimen shown in Fig. 1, and for all specimens in this study, the bottom surface of the laminate is flat to simulate an aerodynamically smooth surface while the top surface changes slope to accommodate the change in thickness. A schematic of the general configuration is shown in Fig. 2. The thick section consists of three sublaminates denoted A, B, and C and the thin section consists of two sublaminates denoted A and C. Sublaminates A and C are identical eight-ply layups of $[+45, -45, 0, 90]_s$. A 0-deg ply is parallel to the x-axis in Fig. 2. Table 1 lists the layups of the dropped plies, also called sublaminate B, considered in this study. A particular test specimen is denoted by the configuration letter shown in Table 1 followed by an integer digit identifying the replicate for that configuration. During fabrication a triangular-shaped pocket of neat resin formed between the end of the dropped plies and sublaminates A and C in the section containing the thickness change (the transition section) for most of the specimens. However, no pocket of neat resin formed for the 90-deg unidirectional dropped-ply layups (configurations F, G, and H in Table 1). For these specimens the material of the 90-deg plies migrated into the transition section during the curing process.

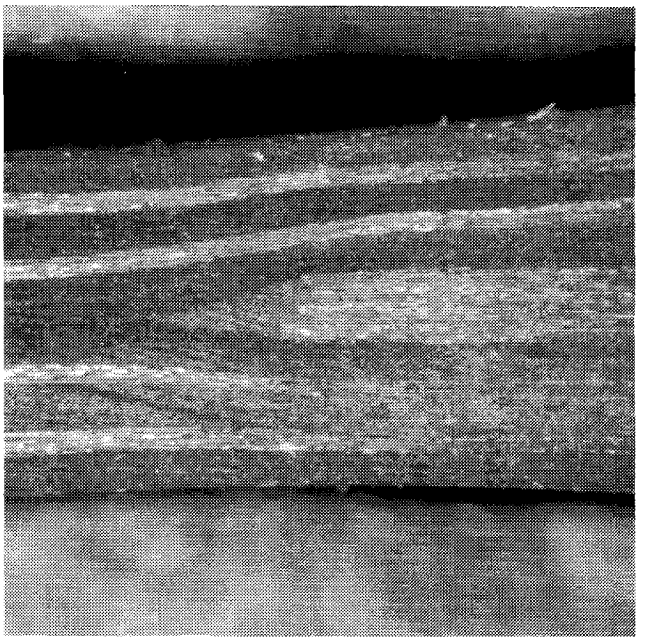

Fig. 1 Photomicrograph of the edge of specimen B4 at $N_x = -6.129$ kN/cm.

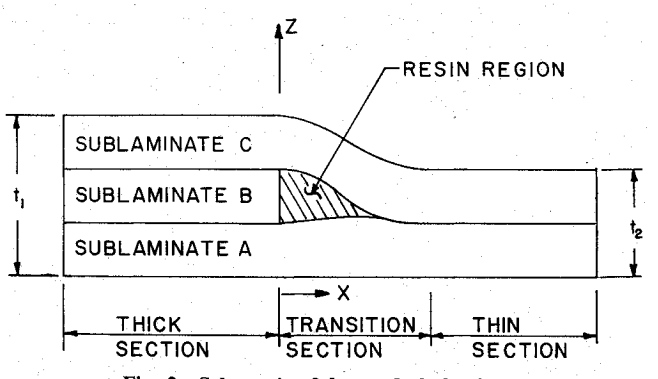

Fig. 2 Schematic of dropped-ply laminate.

Table 1 Laminate configurations

Configuration designation	Sublaminate B: Number of plies	Sublaminate B: Layup	Thickness ratio t_1/t_2
A	2	$[0_2]$	1.125
B	4	$[0_4]$	1.250
C	8	$[0_8]$	1.500
D	8	$[45/-45/0_2]_s$	1.500
E	8	$[45/-45/0/90]_s$	1.500
F	2	$[90_2]$	1.125
G	4	$[90_4]$	1.250
H	8	$[90_8]$	1.500

Specimens that were subjected to tension had fiberglass tabs adhesively bonded to each end to prevent damage from the end grips. The ends of the compression specimens were ground flat and parallel and then mounted in an end-loading fixture. The specimens were tested in flat-end compression using a fixture based on a design shown in Fig. 10 of Ref. 4. The compression fixture clamped 9.53 mm of the specimen in grips at each of the loaded ends to prevent brooming. The unloaded edges of the compression specimens were supported in knife edges to prevent column buckling. Metal shims were used in the thin section to fill the gap between the thin laminate of the specimen and the knife edge supports.

Instrumentation and Tests

Direct current displacement transducers were used to monitor selected out-of-plane displacements and the axial end-shortening for the compression specimens. Moiré interferometry was used to view the out-of-plane displacement. Electrical resistance strain gauges were used to measure strain at selected locations on each specimen.

The compression tests were performed in a 534 kN (120 kip) electrohydraulic test machine under a constant load rate of 8896 N (2000 lbs) per minute until final failure of the specimen. An automatic data acquisition system was used to sample the experimental measurements every 2 s. A Questar telescope with an attached camera was used to observe and photograph the edge of the specimens in the vicinity of the dropped plies during the test. A viewing port was machined in the knife edge supports of the compression test fixture to expose the edge of the specimen. Thus, the development of cracks and delaminations at the free edge in the dropped-ply transition section could be observed and photographed during the loading process.

Analysis

A linear analysis applicable to the 2.54- and 3.81-cm-wide specimens was performed on configurations B and G (sublaminate B layups $[0_4]$ and $[90_4]$, respectively) using two separate finite element computer codes. First, a laminated plate analysis in the x-y plane of the entire test specimen as mounted in the compression test fixture was performed using the

general-purpose computer program STAGS (STructural Analysis of General Shells).[5] The STAGS analysis is referred to herein as the global analysis. The modeling approach used is shown in Fig. 3. The scheme employed for the STAGS model is to use shell units to model the specimens. In this case, shell units 1 and 3 are flat plates for the thick and thin sections, respectively. Shell unit 2 is a short-length, intermediate-thickness plate used in the transition section. Each shell unit was discretized with eight-noded elements having 32 DOF each (element 411 in the STAGS library of elements). The boundary conditions used for the model are also shown in Fig. 3, and these boundary conditions approximate the restraints of the compression test fixture and the applied load.

The second finite analysis is used to model the details of the dropped plies in the transition section. This analysis is based on the generalized plane deformation assumptions of anisotropic elasticity.[2] In this formulation, the displacements contain unknown functions of x and z and explicit polynomial terms to account for uniform stretching, bending, and twisting in the width-wise (y) direction. Hence, the boundary value problem is a two-dimensional one in the x-z plane. All six strain components can be nonzero, but the strain components associated with width-wise stretching and bending are prescribed. Portions of the shear strains associated with a uniform twist about the y-axis are also prescribed. This second finite element analysis is referred to as the local analysis, and is used to determine the three-dimensional state of stress in the vicinity of the dropped plies.

The entire local model is shown in Fig. 4. It is 3.18 cm long ($-1.27 \leq x \leq 1.91$). The thick section is 1.27 cm, the transition section is 0.203 cm, and the thin section is 1.70 cm. The boundary conditions prescribed at $x = -1.27$ and $x = 1.91$ are the displacements corresponding to these axial positions from the STAGS solution at $y = 0$. Eight-noded quadrilateral, and six-noded triangular, isoparametric elements are used throughout the model. Each lamina is modeled with one element through the thickness, except for adjacent 90-deg plies in which one element spans two ply thicknesses. All laminae are assumed to have the same thickness of 0.140 mm. The material property data used in both the local and global analyses are given in Table 2.

The experiments indicated a significant amount of strain in the width-wise direction. These effects can be included to a limited extent in the local model through the polynomial terms

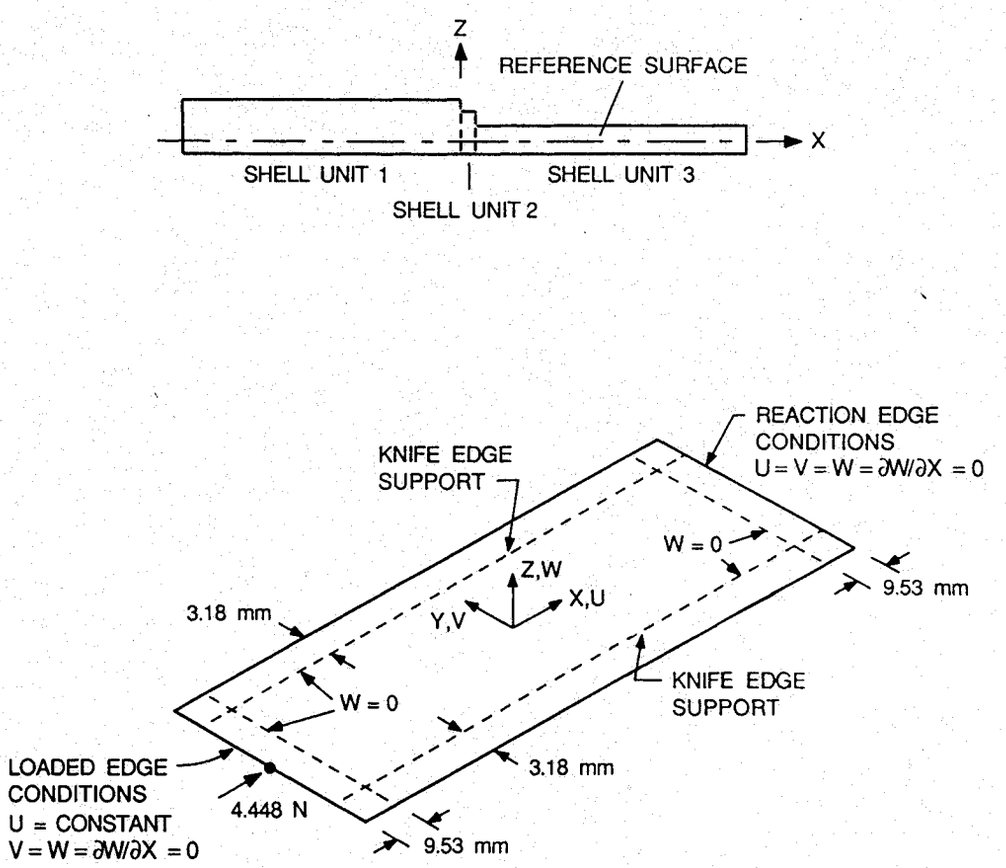

Fig. 3 STAGS modeling of a compression test specimen.

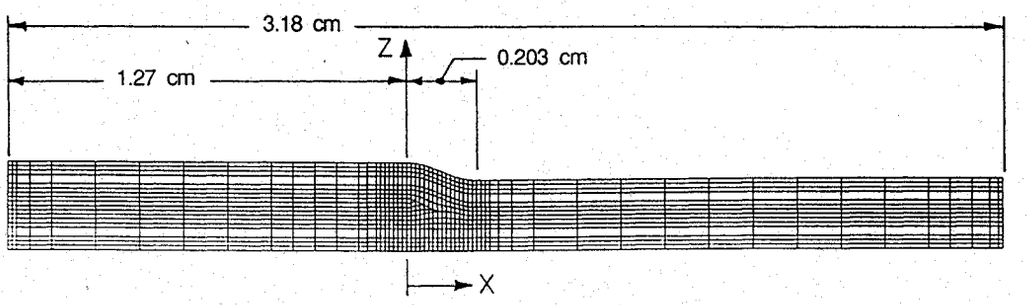

Fig. 4 Finite element model for the local analysis.

in the displacements for the generalized plane deformation analysis. The displacements from generalized plane deformation are taken in the following form for the local model:

$$u = (1/2)\kappa_{xy}yz + U(x, z) \quad (1)$$

$$v = \kappa_y yz + \varepsilon_y^0 y + V(x, z) \quad (2)$$

$$w = -(1/2)\kappa_y y^2 - (1/2)\kappa_{xy}xy + W(x, z) \quad (3)$$

in which ε_y^0, κ_y, and κ_{xy} are prescribed spatial constants accounting for width-wise normal strain, width-wise curvature, and twist-curvature, respectively. The six-by-one strain vector computed from these displacements is

$$\varepsilon = \varepsilon^0 + \bar{\varepsilon} \quad (4)$$

where

$$\varepsilon^T = [\varepsilon_x, \varepsilon_y, \varepsilon_z, \gamma_{yz}, \gamma_{zx}, \gamma_{xy}] \quad (5)$$

$$\varepsilon^{0T} = [0, \varepsilon_y^0 + z\kappa_y, 0, -(x/2)\kappa_{xy}, 0, (z/2)\kappa_{xy}] \quad (6)$$

$$\bar{\varepsilon}^T = [\partial U/\partial x, 0, \partial W/\partial z, \partial V/\partial z, \partial W/\partial x + \partial U/\partial z, \partial V/\partial x] \quad (7)$$

Table 2 Material property data

(A) AS4/3502 graphite-epoxy unidirectional tape[a]	
Moduli of elasticity	E_1 = 128 GPa $E_2 = E_3$ = 11.3 GPa
Poisson's ratios	$\nu_{12} = \nu_{13}$ = 0.3, ν_{23} = 0.35
Shear moduli	$G_{12} = G_{13}$ = 6.0 GPa G_{23} = 3.38 GPa
Fiber tensile strength	X_t = 1.45 MPa
Fiber compressive strength	X_c = −1.45 MPa
Transverse tensile strength	$X_t = Z_t$ = 52 kPa
Transverse compressive strength	$Y_c = Z_c$ = −206 kPa
Shear strengths	$S_{12} = S_{13} = S_{23}$ = 93 kPa
(B) Neat resin (intermediate modulus/low strength from Ref. 11)	
Elastic modulus	3.45 GPa
Poisson's ratio	0.41
Shear modulus	1.34 GPa
Tensile strength	48.3 kPa
Compressive strength	−145 kPa

[a] G_{23} and ν_{23} from Ref. 3; X_t, X_c, Y_t, Y_c, and S_{12} from Ref. 10 for AS/3501; Z_t, Z_c, S_{13}, and S_{23} assumed.

The width-wise normal strain, curvature, and twist-curvature are determined from the STAGS solution. However, in the STAGS solution the strain ε_y^0 and curvatures κ_y and κ_{xy} vary with x for $y = 0$, and are not spatially constant. Although it violates the elasticity formulation given in Ref. 2, it is assumed that these quantities are piecewise constant from element to element in the local analysis. The mathematical formulation of the local finite element model is based on stationarity of the potential energy: The strains in Eqs. (4–7) are substituted into the strain energy, and the unknown portions of the displacements $U(x, z)$, $V(x, z)$, and $W(x, z)$ are represented in the usual fashion of the finite element method. In the formulation, the prescribed width-wise strain terms in Eq. (6) lead to a distributed initial force intensity vector acting at every node in the mesh. This prescribed initial force intensity vector approximates the width-wise effects in the solution plane. See Refs. 6 and 7 for further details.

Results and Discussion

Experimental

The response of the 2.54- and 3.81-cm-wide specimens was linear to initial failure, and these specimens are strength-critical specimens. The 7.62-cm-wide specimens buckled in compression, and exhibited a geometrically nonlinear response. The experimental data for the 7.62-cm-wide specimens are given in Ref. 6.

The average values of N_x at the initiation of damage and at the ultimate load for each dropped-ply configuration, and for tension and compression, are given in Table 3. The scatter in the data for a given configuration and sense of the load is indicated by the coefficient of variation in the table. For configurations A through E the ultimate strength is higher for tension than compression by 20–35%. The additional load carrying capacity after initial failure is also much higher for tension than compression, e.g., 1.90–5.29 kN/cm for tension versus 0–0.98 kN/cm for compression. Thus, compression is more critical than tension, and the majority of the discussion in this paper is on the former rather than the latter.

Using the Questar telescope and camera arrangement, photomicrographs of the compression specimens' edges were taken during the failure process. Photomicrographs just prior to failure initiation and just after the first major failure event

Table 3 Failure loads for strength-critical specimens

		Failure loads[a]			
		Initial		Ultimate	
Specimens	Dropped-ply layup	Average kN/cm	COV,[b] %	Average kN/cm	COV[b], %
A1, A2	$[0_2]$	7.531	—	12.82	2.5
A3, A4, A5, A6	$[0_2]$	−9.044	2.4	−9.331	3.7
B1, B2	$[0_4]$	9.018	4.1	11.50	6.4
B3, B4, B5	$[0_4]$	−6.415	1.8	−7.392	3.0
C1, C2	$[0_8]$	8.126	7.3	9.776	—
C3, C4, C5, C6	$[0_8]$	−6.009	5.8	−6.221	4.1
D1, D2	$[\pm 45/0_2]_s$	7.443	1.7	9.672	2.3
D3, D4, D5	$[\pm 45/0_2]_s$	−6.879	3.7	−6.917	3.9
E1, E2	$[\pm 45/0/90]_s$	7.530	3.3	9.425	0.16
E3, E4, E5	$[\pm 45/0/90]_s$	−7.716	4.4	−7.716	4.4
F1, F3, F4	$[90_2]$	−10.91	6.5	−10.91	6.5
G1, G3, G4	$[90_4]$	−12.46	8.0	−12.46	8.0
H1, H3, H4, H5	$[90_8]$	−11.75	9.1	−11.75	9.1

[a] Positive loads are from tension tests, and negative loads are from compression tests.
[b] COV is the coefficient of variation in percent (= 100 × (std. dev.)/average).

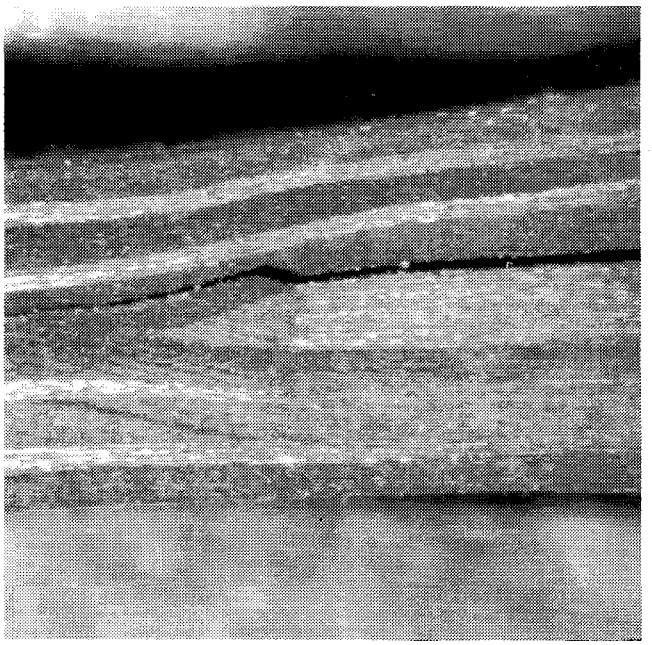

Fig. 5 Photomicrograph of the edge of specimen B4 at $N_x = -6.304$ kN/cm.

for specimen B4 are shown in Figs. 1 and 5. Failure initiation is characterized by the sudden appearance of a large crack at a compressive load of −6.304 kN/cm as shown in Fig. 5. The occurrence of this first failure could not be detected visually (Fig. 1) or by the strain gauge response. The difference in the compressive load between Figs. 1 and 5 is only −175.1 N/cm. The exact location of the initiation of the large crack in Fig. 5 is not evident, but it is thought to originate at the intersection of the resin-rich region and sublaminates B and C. From this point the crack shears across the +45-deg ply of sublaminate C and propagates along the +45/−45 interface into the thin section. Propagation in the thick section occurs along the interface between sublaminates B and C. The ultimate failure for the compression specimens of configurations A through E is characterized by local crushing of the laminate in a region adjacent to the dropped-ply location. At the ultimate load for specimen B4 sublaminates A and C completely failed at the dropped-ply location, and the dropped plies are driven in a wedge-like manner into the thin section splitting the interface between sublaminates A and C.

The failure of configurations F, G, and H (sublaminates B layups $[90_2]$, $[90_4]$, and $[90_8]$, respectively) occurred within the end grips in the thin section. The ultimate strength of these specimens may be higher, and whether failure would have occurred at the dropped-ply location is uncertain. As can be determined from Table 3, the experimental scatter in the failure loads is larger for the configuration F, G, and H specimens than for the other configurations. This scatter is probably due in part to the failure of these specimens in the end grips. Specimen H5 is an exception, because it failed in the transition section.

To assess the reduction in the compression strength caused by the dropped plies, the strength of the 16-ply quasi-isotropic laminate in the thin section was individually measured. Since all dropped-ply specimens have the same layup in the thin section, the strength of the thin section provides a common reference for the strength of all dropped-ply specimens. Constant-thickness coupons 2.54-cm square were cut from the thin section of two test specimens. Compression tests of the coupons were conducted in an end-loading fixture that gripped 9.53 mm of the coupon at each end. One coupon failed in the grip due to end brooming at −13.31 kN/cm, and the other failed in the test section at −12.61 kN/cm. Assuming the lower strength magnitude to be representative for the thin section, it is clear from the compression strength data in Table 3 that dropped plies can cause a significant reduction in compressive strength. For example, specimen A3, which contains two dropped plies had an ultimate compressive failure load of −9.807 kN/cm, and this represents a 22.2% reduction from −12.61 kN/cm.

The failure loads for the compression specimens are summarized in Fig. 6, which shows the influence of the number of dropped plies and their layup on compression strength. In Fig. 6 the compressive load intensity at failure is plotted versus the thickness ratio t_1/t_2, where t_1 is the thickness of the thick section and t_2 is the thickness of the thin section. The filled circle labeled "constant-thickness specimen" is the compression strength (−12.61 kN/cm) of the thin section measured from the constant-thickness coupon test. The open square symbols indicate the average strengths of all replicate test specimens for a given sublaminate B layup. It is clear from this figure that the presence of dropped plies reduces the compressive strength of the laminate below that of its thin section. For the 0-deg sublaminate B layups, the strength decreases as the number of dropped plies increases from two to eight. However, for the 90-deg sublaminate B layups, the strength does not change significantly as the dropped plies are increased from two to eight. Also, the data for a thickness ratio of 1.5 illustrate that the compression strength increases as the axial stiffness of the dropped plies decreases.

The results in Fig. 6 suggest that the change in axial stiffness between the thick and thin sections has a strong influence on compression strength. This observation is substantiated in Table 4, in which the strength ratio and compliance ratio are tabulated for each configuration from test data. The strength ratio is defined as the compression strength of the thin section divided by the compression strength of the dropped-ply specimen. The compliance ratio is defined as the axial compliance of the thin section divided by the axial compliance of the thick section. The compliance ratio is obtained from test data by dividing the far-field axial strain in the thin section by the far-field axial strain in the thick section at a fixed value of the load. The correlation of these two ratios in Table 4 demonstrates that the reduction in compression strength of the dropped-ply specimens varies directly with the reduction in axial compliance of the thick section relative to the thin section.

Analytical

The compression tests on specimens B4 and G1 were analyzed using the global/local finite element codes discussed

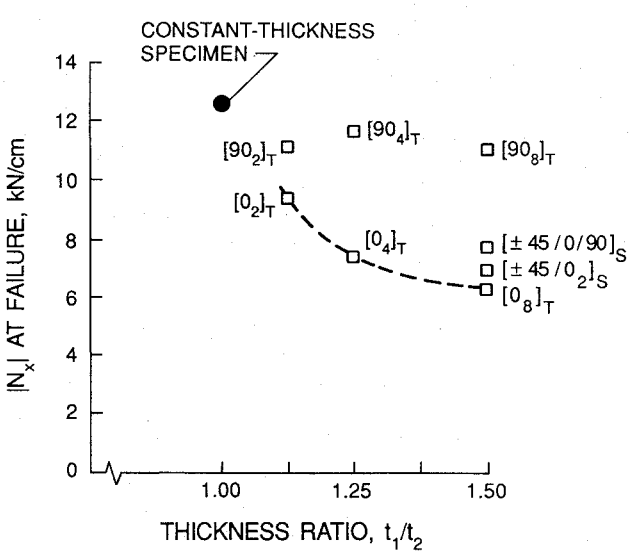

Fig. 6 Failure load intensity vs thickness ratio for the compression specimens.

Table 4 Correlation of the compression strength and compliance ratio

Dropped-ply configuration[a]	Strength ratio[b]	Compliance ratio[c]
A	1.3512	1.3157
B	1.7062	1.6762
C	2.0265	2.3565
D	1.5929	1.5242
E	1.8677	1.7666
F	1.1555	1.0630
G	1.0155	0.9959
H	1.0285	1.1583

[a]See Table 1 for laminate description.
[b]Compression strength of the thin section (12.61 kN/cm) determined from coupon test divided by the compression strength of the dropped-ply laminate.
[c]Axial compliance of the thin section divided by axial compliance of the thick section.

above. Specimen B4 had four 0-deg plies terminated, was 2.54 cm wide, and failure initiated at $N_x = -6.303$ kN/cm with ultimate failure at -7.587 kN/cm. Specimen G1 had four 90-deg plies terminated, was 3.81 cm wide, and failed at $N_x = -11.62$ kN/cm. The failure of specimen B4 was at the ends of the dropped plies, and specimen G1 failed in the end grip of the thin section.

The axial strain distributions along the top and bottom surfaces of specimen B4 for $N_x = -1.751$ kN/cm are shown in Fig. 7. The filled circular symbols are the strain gauge readings on the top surface, and the unfilled square symbols are the strain gauge readings on the bottom surface. The dotted line is the top surface strain from the local analysis, and the solid line the bottom surface strain. The nearly identical strain gauge readings for the top and bottom surfaces at $x = -2.54$ cm and $x = 2.54$ cm indicate that the specimen is essentially subjected to pure compression in regions removed from the dropped-ply location. Since the thick section is stiffer than the thin section, the magnitude of the strains at $x = -2.54$ is less than that of the strains at $x = 2.54$.

The correlation between the experiment and analysis for the top surface strains in Fig. 7 is quite good. The top surface strains in the transition section were not computed, so the apparent jump in top surface strain at $x = 0$ in Fig. 7 is actually a continuous and rapidly changing quantity. No strain gauges were mounted on the top surface of the test specimen in the transition section to establish a data point in this region of rapid change. The correlation between the experiment and analysis for the bottom surface strains is reasonable except near $x = 0$. Here the analytical distribution exhibits an oscillation about the experimental strain data. The plots of the top and bottom surface strain distributions intersect in the thin section in the vicinity of $x = 1.27$ cm. This intersection implies a reversal in the bending moment in the thin section. However, a reversal of the bending moment near $x = 1.27$ cm did not occur in the experiment, nor did it occur in the global STAGS solution. No reason for the moment reversal in the thin section of the local analysis was determined.

The axial strain distributions for the top and bottom surfaces for specimen G1 are shown in Fig. 8 for $N_x = 1.751$ kN/cm. The strain gauge readings at $x = -2.54$ cm and $x = 2.54$ cm do not differ by very much, indicating that the 90-deg plies in sublaminate B do not increase the stiffness of the thick section relative to the thin section very much. The correlation between the experiment and analysis is good.

Failure Analysis

The first major failure event for the 0-deg sublaminate B dropped ply specimens was a delamination in the upper interface between the dropped plies (sublaminate B) and sublaminate C (see Fig. 5). To study delamination requires a means to compute the interlaminar stresses and a criterion to predict it. The main purpose in the development of the local analysis code was to compute the interlaminar stresses. The delamination failure criterion employed in this study was taken from Ref. 8.

Plots of the scaled interlaminar normal and shear stresses along the upper and the lower interface of the dropped plies for the $[0_4]$ dropped-ply layup are shown in Figs. 9 and 10, respectively. The interlaminar stresses are divided by the average compressive normal stress in the thin section, $-N_x/t_2$. The interlaminar normal stress attains its maximum tensile value in the upper interface (dashed line) at the dropped-ply location ($x = 0$), and decays rapidly to zero along the interface into the thick section. The magnitudes of the interlaminar normal stress are smaller in the lower interface (solid line) than the tensile peak value in the upper interface. The interlaminar shear stress also attains its maximum value in the upper interface as shown in Fig. 10, but the maximum magnitude occurs at a value of x slightly less than zero. The interlaminar shear stress decays more slowly than the normal stress component along the upper interface in the thick section.

The interlaminar stress distribution plots for the $[90_4]$ sublaminate B layup are shown in Figs. 11 and 12, and are anal-

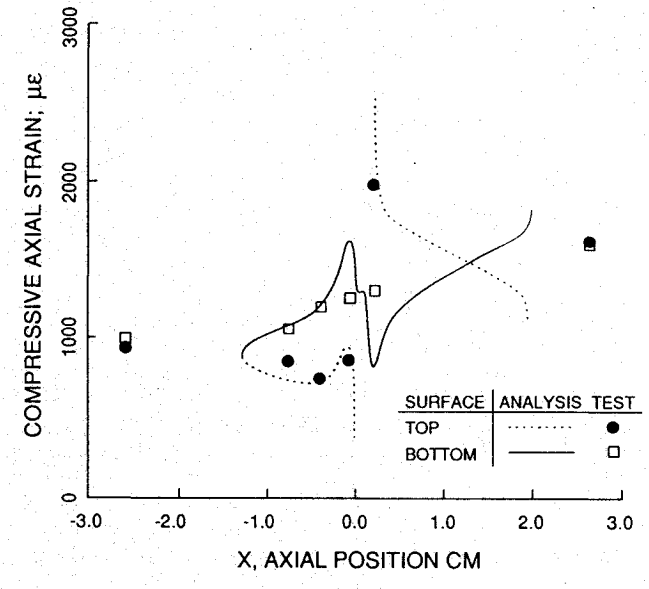

Fig. 7 Axial strain distributions for specimen B4 at $N_x = -1.751$ kN/cm.

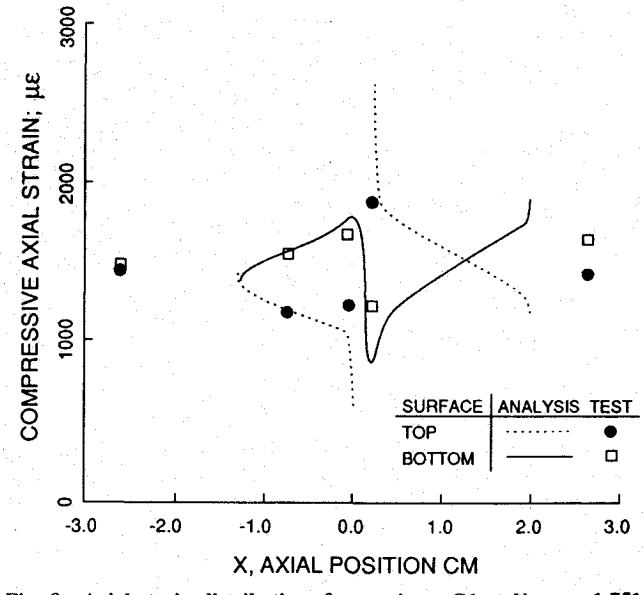

Fig. 8 Axial strain distributions for specimen G1 at $N_x = -1.751$ kN/cm.

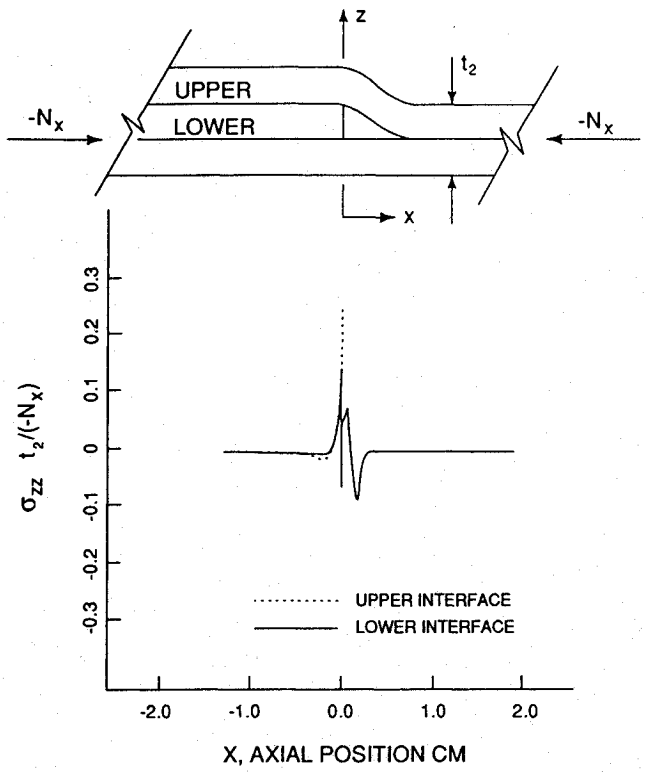

Fig. 9 Interlaminar normal stress distribution for the [0₄] sublaminate B configuration.

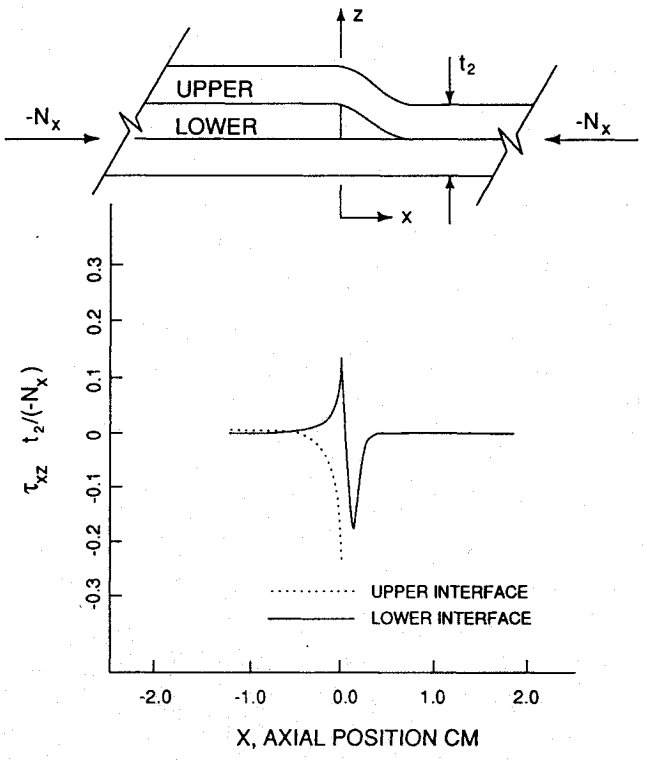

Fig. 10 Interlaminar shear stress distribution for the [0₄] sublaminate B configuration.

ogous to Figs. 9 and 10, respectively, for the [0₄] sublaminate B layup. The peak tensile interlaminar normal stress for the [90₄] configuration shown in Fig. 11 occurs in the upper interface at $x = 0$, but is about 50% of the peak normal stress for the [0₄] configuration shown in Fig. 9. Also, the interlaminar shear stresses in the upper interface for the [90₄] configuration shown in Fig. 12 are negligible compared to corresponding shear stresses of the [0₄] configuration shown in Fig. 10. These lower interlaminar stress magnitudes may be the reason why the [90₄] configuration is less delamination prone in the dropped-ply region that the [0₄] configuration.

The delamination criterion, or the tensile interlaminar failure mode criterion, used in this study is

$$(\sigma_{zz}/Y_t)^2 + (\sigma_{zx}^2 + \sigma_{zy}^2)/S_{23}^2 = 1; \qquad \sigma_{zz} > 0 \qquad (8)$$

The strength values for the material are given in Table 2. This criterion is a modification of the intralamina tensile matrix mode criterion given by Hashin in Ref. 9. The modification of the intralamina criteria to an interlaminar one is accomplished by neglecting the noninterlaminar stress components. The criterion, Eq. (8), was evaluated at all interfaces between plies with different fiber orientations in the local model. The criterion was found to be a maximum in the upper interface of the dropped plies at $x = 0$ for both specimens B4 and G1. Thus, the delamination criterion predicted the correct location of failure initiation for specimen B4. The predicted failure load intensity for specimen B4 was $N_x = -4.215$ kN/cm, and this is 67% of the experimental failure initiation load of -6.303 kN/cm. The predicted failure load intensity for specimen G1 was $N_x = -6.971$ kN/cm, and this is 60% of the experimental failure load of -11.61 kN/cm. The failure load was also underestimated for specimen G1. Since specimen G1 failed in the grip and not in the test section, it is probable that the experimental failure load would be larger in magnitude if failure was initiated by delamination in the dropped-ply region. Thus, the predicted delamination failure load for specimen G1 would be less than 60% of the experimental delamination failure load if the latter could be achieved.

Intralamina modes of failure were also evaluated in this study. These modes were evaluated by the quadratic tensor polynomial criterion[10] and the individual modal criteria presented by Hashin.[9] For the [0₄] sublaminate B layup the tensor polynomial criterion predicted first-ply failure in the top 0-deg dropped ply near $x = 0$. The predicted failure load was $N_x = -1.972$ kN/cm. Hashin's tensile matrix mode criterion predicted the same location of failure as the tensor polynomial criterion but the failure load was $N_x = -1.851$ kN/cm. The agreement of these two criteria implies that matrix splitting in the dropped plies is the first failure event. If this did occur in the configuration B specimens, it was not detected by the instrumentation used in the experiments.

For the [90₄] sublaminate B layup, the tensor polynomial criterion and the tensile matrix mode criterion predicted the same location for first ply failure, which was in the lower 0-deg ply in the transition section of sublaminate C. The failure load for the tensor polynomial criterion was $N_x = -6.591$ kN/cm, and the failure load for the tensile matrix mode criterion was $N_x = -7.779$ kN/cm. All the other intralamina failure mode criteria presented by Hashin in Ref. 9 predicted failure loads in excess of the delamination criterion.

Concluding Remarks

The results of this study show that both the tensile and compressive strengths may be significantly reduced by the presence of the thickness discontinuity. The reduction in compression strength is greater than the reduction in tensile strength for a given configuration. In all cases studied the compression strength of the dropped ply laminate is less than the compression strength of its thin section. Analysis of the experimental data showed the reduction in strength is directly related to the increase in the axial stiffness of the thick section relative to the thin section. Thus, the greater the change in stiffness between the thick section and the thin section at the dropped-ply location, the greater is the reduction in strength.

The first major failure event for the specimens with 0-deg dropped-ply layups was a delamination at the upper interface of the dropped plies. The delamination appeared to initiate

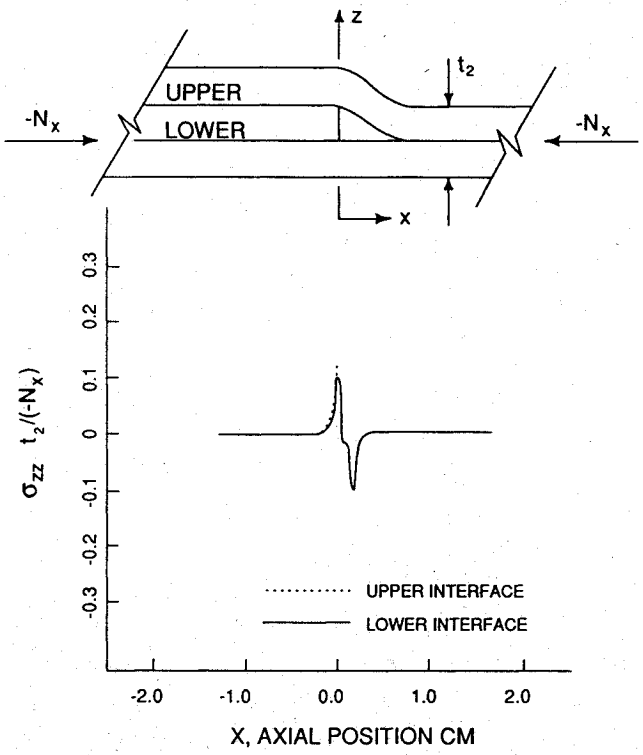

Fig. 11 Interlaminar normal stress distribution for the $[90_4]$ sublaminate B configuration.

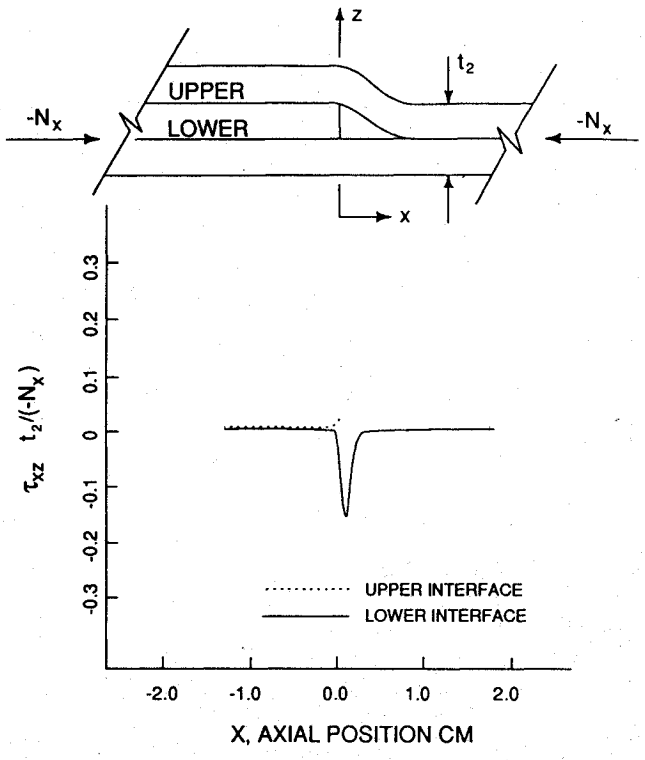

Fig. 12 Interlaminar shear stress distribution for the $[90_4]$ sublaminate B configuration.

at the end of the dropped ply adjacent to the upper interface. The interlaminar failure criterion used in the analysis also predicted the location of failure initiation in the upper interface at the end of the dropped plies. However, the failure analysis underestimated the experimental compressive failure load by 33%, which results in a conservative analysis procedure for structural design.

The analysis showed the interlaminar normal stress in the upper interface of the dropped plies is a maximum at the end of the dropped plies, and at the same location the interlaminar shear stress is close to its maximum value. Both the interlaminar normal stress and shear stress decay to zero along the upper interfaces, but the former decays more rapidly than the latter. Also, both components of stress are the same order of magnitude in the upper interface. Since the interlaminar normal strength is about one-half of the interlaminar shear strength (see Table 2), the failure criterion, Eq. (8), is more sensitive to the normal stress component than to the shear stress components. At failure, the term in Eq. (8) containing the interlaminar normal stress accounted for 95% of the total. The relatively large contribution of the interlaminar normal stress term compared to the shear stress terms in Eq. (8) suggests delamination is primarily initiated by the interlaminar normal (peeling) stress. The fact that the interlaminar shear stresses do not appear to be very significant contributors to delamination is interesting, since the transfer of the axial load to the dropped plies is by interlaminar shear.

The analytical results supported the trend observed in the experiments that the compression strength increases as the axial stiffness of the dropped plies decreases. The predicted strength of the laminate with a $[90_4]$ dropped-ply layup is greater than the predicted strength of the laminate with a $[0_4]$ dropped-ply layup.

Acknowledgment

The first two authors gratefully acknowledge the support for their work in this research by the NASA Langley Research Center under Grant NAG-1-537.

References

[1]Kemp, B. L., and Johnson, E. R., "Response and Failure Analysis of a Graphite-Epoxy Laminate Containing Terminating Internal Plies," *Proceedings of the AIAA/ASME/ASCE/AHS 26th Structures, Structural Dynamics, and Materials Conference*, Pt. 1, AIAA, New York, April 1985, pp. 13–24; AIAA Paper 85-0608.

[2]Lekhnitskii, S. G., *Theory of Elasticity of an Anisotropic Body*, English translation, Mir Publishers, Moscow, 1981, pp. 99–105.

[3]Adams, D. F., Ramkumar, R. L., and Walrath, D. E., "Analysis of Porous Laminates in the Presence of Ply Drop-Offs and Fastener Holes," Northrop Technical Rept. NOR 84-113, Northrop Corp., Hawthorne, CA, and Univ. of Wyoming, Laramie, WY, May 1984.

[4]"NASA/Aircraft Industry Standard Specification for Graphite Fiber/Toughened Thermoset Resin Composite Material," NASA RP-1142, June 1985.

[5]Almroth, B. O., Brogan, F. W., and Stanley, G. W., "User's Manual for STAGS," NASA Contractor Rept. 165670, March 1978, Vols. 1 and 2.

[6]Curry, J. M., Johnson, E. R., and Starnes, J. H., Jr., "Effect of Ply Drop-Offs on the Strength of Graphite-Epoxy Laminates," Center for Composite Materials and Structures Rept. CCMS 86-07 and College of Engineering Rept. VPI-E-86-27, Virginia Polytechnic Inst. and State Univ., Blacksburg, VA, Dec. 1986.

[7]Curry, J. M., Johnson, E. R., and Starnes, J. H., Jr., "Effect of Dropped Plies on the Strength of Graphite-Epoxy Laminates," *Proceedings of the AIAA/ASME/ASCE/AHS 28th Structures, Structural Dynamics and Materials Conference*, AIAA, Washington, DC, April 1987, p. 737; AIAA Paper 87-0874.

[8]Rosen, B. W., Nagarkar, A. P., Pipes, R. B., and Walsh, R., "Research Study to Define the Critical Failure Mechanisms in Notched Composites Under Compression Fatigue Loading," Materials Science Corp. Rept. MSC TFR 1201/1801, Contract N00019-79-C-0633, March 1981, pp. 5–8 and 33–45.

[9]Hashin, Z., "Failure Criteria for Unidirectional Fiber Composites," *Journal of Applied Mechanics*, Vol. 47, June 1980, pp. 329–334.

[10]Tsai, S. W., *Composits Design–1985*, Think Composites, Dayton, OH, 1985, pp. 10-5, 10-6, and 10-12.

[11]Chamis, C. C., "Simplified Composite Micromechanics Equations for Hygral, Thermal, and Mechanical Properties," *SAMPE Quarterly*, April 1984, pp. 14–23.